Physicochemical properties and cellular toxicity of (poly)aminoalkoxysilanes-functionalized ZnO quantum dots

2012 Nanotechnology 23 335101

(http://iopscience.iop.org/0957-4484/23/33/335101)

Nanotechnology **23** (2012) 335101 (9pp) doi:10.1088/0957-4484/23/33/335101

Physicochemical properties and cellular toxicity of (poly)aminoalkoxysilanes-functionalized ZnO quantum dots

Abdelhay Aboulaich[1], Carmen-Mihaela Tilmaciu[1], Christophe Merlin[2], Cédric Mercier[3], Hélène Guilloteau[2], Ghouti Medjahdi[3] and Raphaël Schneider[1]

[1] Laboratoire Réactions et Génie des Procédés (LRGP), UPR 3349, CNRS-Université de Lorraine, 1 rue Grandville, F-54001 Nancy Cedex, France
[2] Laboratoire de Chimie Physique et Microbiologie pour l'Environnement (LCPME), UMR 7564, CNRS-Université de Lorraine, 15 Avenue du Charmois, F-54500 Vandoeuvre-lès-Nancy, France
[3] Institut Jean Lamour (IJL), UMR 7198, CNRS-Université de Lorraine, BP 70239, F-54506 Vandoeuvre-lès-Nancy Cedex, France

E-mail: raphael.schneider@univ-lorraine.fr

Received 28 March 2012, in final form 14 June 2012
Published 3 August 2012
Online at stacks.iop.org/Nano/23/335101

Abstract
Luminescent ZnO nanocrystals were synthesized by basic hydrolysis of $Zn(OAc)_2$ in the presence of oleic acid and then functionalized with (poly)aminotrimethoxysilanes in the presence of tetramethylammonium hydroxide to render the QDs water-dispersible. The highest photoluminescence quantum yield (17%) was achieved using N_1-(2-aminoethyl)-N_2-[3-(trimethoxysilyl)propyl]-1,2-ethanediamine as surface ligand. Transmission electron microscopy and powder x-ray diffraction showed highly crystalline materials with a ZnO nanoparticle diameter of about 4 nm. The cytotoxicity of the different siloxane-capped ZnO QDs towards growing *Escherichia coli* bacterial cells was evaluated in MOPS-minimal medium. Although concentrations of 5 mM in QDs caused a complete growth arrest in *E. coli*, siloxane-capped ZnO QDs appeared weakly toxic at lower doses (0.5 or 1 mM). The concentration of bioavailable Zn^{2+} ions leaked from ZnO QDs was evaluated using the biosensor bacteria *Cupriavidus metallidurans* AE1433. The results obtained clearly demonstrate that concentrations of bioavailable Zn^{2+} are too low to explain the inhibitory effects of the ZnO QDs against bacteria cells at 1 mM and that the siloxane shell prevents ZnO QDs from dissolution contrary to uncapped ZnO nanoparticles. Because of their low cytotoxicity, good biocompatibility, low cost and large number of functional amine end groups, which makes them easy to tailor for end-user purposes, siloxane-capped ZnO QDs offer a high potential as fluorescent probes and as biosensors.

S Online supplementary data available from stacks.iop.org/Nano/23/335101/mmedia

(Some figures may appear in colour only in the online journal)

1. Introduction

Semiconductor nanocrystals (quantum dots, QDs) with narrow size distribution and high luminescence efficiency have attracted the attention of researchers due to their wide applications as biological labels, sensors, light-emitting diodes (LEDs), and lasers [1–7]. Low band gap II–VI and IV–VI semiconductors such as CdSe and CdTe have been intensively studied in the form of size- and shape-controlled nanocrystals during the past decade, especially for biological labeling [8–14]. However, despite their appealing optical properties, the intrinsic toxicity of cadmium and

the production of reactive oxygen species (ROS) [15, 16] from these nanocrystals has shed a doubt on the future applicability of Cd-containing QDs, particularly in view of recent environmental regulations.

Considering the problems associated with heavy metal ion-based QDs, the search for Cd-free QDs has become increasingly important and constitutes the most challenging aspect of working with these materials in biological and medical fields. Zinc oxide ZnO is a promising alternative to Cd-containing QDs, which pose a much higher risk to biological systems than Zn-based QDs. ZnO has a direct band gap (band gap of 3.37 eV at room temperature) with a relatively high exciton binding energy (60 meV) which has found various applications in optical, electronic, and sensing devices [17, 18]. ZnO QDs have only scarcely been used for cell labeling applications due to the modest stability of ZnO nanocrystals in water [19, 20], especially at low pH since water molecules can attack their luminescent centers on the ZnO surface and destroy them rapidly [21].

In the last few years, various strategies have been developed to stabilize and disperse ZnO QDs in aqueous media. Embedding ZnO QDs in poly(methacrylate)/poly(ethyleneglycol) copolymers [22, 23] or with poly(ethyleneimine) [24] has successfully been used to disperse these nanocrystals in water with preservation of their fluorescent properties. Encapsulation of ZnO QDs with silica to form ZnO@silica core/shell nanoparticles has also recently been described to obtain ZnO QDs with good water stability [25]. An alternative and interesting methodology for surface functionalization and stabilization of ZnO nanocrystals is based on organosilanes' chemistry to inhibit decomposition in aqueous media. Since the first report of ZnO nanoparticles' surface modification with silane [26], this strategy has successfully been used for the stabilization of ZnO QDs in water. Trialkoxysilanes have a strong affinity with hydroxylated surfaces, form covalent bonds with them, thereby creating a shielding barrier of cross-linked polysiloxanes that protects the nanocrystal at the core [21, 27–34]. In recent studies, we have demonstrated the advantages of using poly(ethyleneglycol)siloxane [35] and siloxane-core poly(amidoamine) dendrons [36] to transfer hydrophobic oleate-capped ZnO QDs in water with preservation of their luminescent properties.

The aims of this study were to investigate the efficiency of (poly)aminosilanes as capping agents of ZnO QDs in terms of stabilization and dispersion, and to address the toxicity of these QDs, since all these parameters are of critical importance for bio-imaging studies and sensor applications. For that purpose, ZnO nanoparticles were functionalized with 3-aminopropyltrimethoxysilane (APTMS), *N*-(2-aminoethyl)aminopropyltrimethoxysilane (AEAPS), or N_1-(2-aminoethyl)-N_2-[3-(trimethoxysilyl)propyl]-1,2-ethanediamine (AETPE) (figure 1). Surface modified ZnO QDs were characterized by transmission electron microscopy, powder x-ray diffraction, dynamic light scattering, zeta potential measurements, and UV–vis and fluorescence spectroscopies. The effect of structural properties of the (poly)aminosilanes on the formation, stabilization, photoluminescence properties, and cytotoxicity of ZnO nanoparticles have been evaluated. Growth inhibition tests showed that aminosiloxane-capped ZnO QDs did not prevent *E. coli* cells from growing before concentrations as high as 5 mM and that Zn^{2+} ion leakage from the nanocrystals is not the primary source of the toxicity observed as determined by specific metal-sensing bacteria.

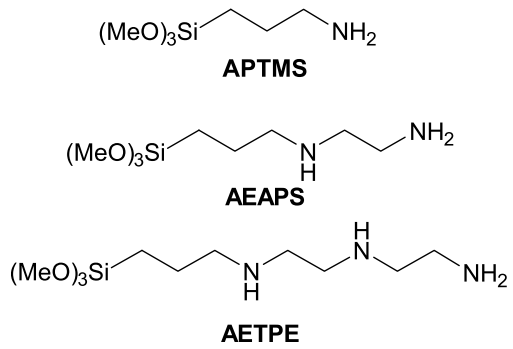

Figure 1. Structures of aminosilanes used for QD surface functionalization.

2. Experimental section

2.1. Reagents and materials

Anhydrous zinc acetate (Aldrich), oleic acid (Aldrich), tetramethylammonium hydroxide [TMAH] (Aldrich), 3-aminopropyltrimethoxysilane [APTMS] (Acros Organics), *N*-(2-aminoethyl)aminopropyltrimethoxysilane [AEAPS] (Aldrich), 3-[2-(2-aminoethylamino)ethyl-amino]propyl-trimethoxysilane [AETPE] (Acros Organics), anhydrous toluene and ethanol (HPLC grade) were used as-received without additional purification. All aqueous solutions were prepared using Milli-*Q* water (18.2 MΩ cm, Millipore).

2.2. Synthesis of oleate-capped ZnO QDs

Zinc acetate (220 mg, 1.2 mmol) was dissolved in ethanol (20 ml) at a temperature below 50 °C under vigorous stirring. Oleic acid (70 μl, 0.22 mmol) was then added and the mixture was heated to reflux. In a separate flask, tetramethylammonium hydroxide (360 mg, 1.99 mmol) was dissolved in refluxing ethanol (5 ml). This solution was then rapidly injected into the flask containing $Zn(OAc)_2$ and oleic acid, and the mixture was refluxed for 2 min. The mixture was then diluted with ethanol (50 ml) and cooled down to 0 °C with an ice bath. The resulting turbid solution of ZnO nanoparticles was then centrifuged (15 min at 4000 rpm) with removal of the supernatant and washed several times with ethanol, in which they are insoluble. The collected precipitate was finally dispersed in 10 ml of toluene leading to a clear oleate-capped ZnO QDs dispersion.

2.3. Synthesis of aminosiloxane-capped ZnO QDs

Under a nitrogen atmosphere, the oleate-capped ZnO QDs previously prepared were dispersed in toluene (10 ml) and

mixed with 2 ml of a 0.1 M aminosilane solution in toluene. 2 ml of a 0.1 M solution of TMAH in ethanol were then added and the temperature was set at 85 °C. After 15 min, the solution was allowed to cool and nanoparticles isolated by centrifugation (4000 rpm, 15 min). After removal of the supernatant, the precipitate was washed three times with toluene to remove the oleate ligand. The modified ZnO QDs were redispersed in toluene (10 ml) and 4 ml of 0.1 M TMAH solution were added. The reaction mixture was heated to 85 °C for 30 min. The resulting aminosiloxane-capped ZnO QDs were isolated by centrifugation (4000 rpm, 15 min), washed three times with ethanol, and dried in vacuum (30 mm Hg, 3 h, room temperature) before use.

2.4. Ninhydrin test

Ninhydrin tests were run to quantify primary amines at the surface of ZnO QDs using the following procedure [37]. A calibration curve was first constructed with leucine, which was dissolved in water. A dispersion of (poly)aminosiloxanes-capped ZnO QDs (2 mg) in 10 ml water was combined with 2.5 ml of ninhydrin (7.5 mM in water). The mixture was heated to reflux for 5 min. After cooling to room temperature and centrifugation (4000 rpm for 10 min), the UV–vis absorbance at 570 nm was measured to determine the number of reactive primary amines relative to the leucine standard.

2.5. Cytotoxicity tests

Bacteria were routinely cultured at 30 °C under agitation (160 rpm) in 250 ml conical flasks filled with 50 ml of MOPS-buffered minimal medium (or RM medium [38]) supplemented with Fe-citrate and trace elements as described by Mergeay *et al* [39] for the 284 medium, and 0.2% gluconate as carbon source. Growth inhibition tests were carried out on *Escherichia coli* MG1655 as previously described [15]. Briefly, bacteria were pre-grown in RM medium without QD until the cultures reached mid-log phase (optical density (OD) at 600 nm around 0.2). Cultures were then diluted one-tenth in pre-warmed RM medium spiked to final QD concentrations of 0.5, 1, or 5 mM and the OD_{600} was measured at intervals. For each growth condition, the doubling times of exponentially growing cultures were calculated from the slope of a regression curve, and compared to the one obtained for control cultures in the same medium without QDs (112 ± 4 min for *E. coli* MG1655).

2.6. Quantification of bioavailable Zn^{2+}

Bioavailable Zn^{2+} leaking from QDs was quantified using the whole cell biosensor *Cupriavidus metallidurans* AE1433, a genetically modified bacteria emitting light when sensing bioavailable Zn^{2+} [38]. Bioluminescence of this sensor bacteria increases proportionally with the concentrations of bioavailable Zn^{2+} in the test medium under non-toxic conditions. For biosensing, strain AE1433 was first cultured in LB until stationary phase was reached ($OD_{600} = 1.5$). Bacterial cells were then washed twice by alternating centrifugation (10 000 g for 2 min at 20 °C) end cell pellet dispersion in RM medium supplemented with 0.01% gluconate. AE1433 cell suspension was adjusted to $OD_{600} = 0.3$ in the same medium, and aliquoted (180 μl) in clear bottom black microtiter plates previously filled with various dilutions (20 μl) of either $ZnCl_2$ for calibration curves, or QDs for testing. Microtiter plates were maintained at 23 °C in a VICTOR^3 multilabel plate reader (Perkin-Elmer), where light emission and OD_{600} were recorded every 30 min, with a 5 s and 1 s measurement time respectively, preceded by a 10 s double orbital shaking. For both parameters, background provided by RM-gluconate medium was subtracted, and luminescence was normalized to the corresponding OD_{600}. Normalized luminescence values were averaged among duplicates and induction factors were calculated for each time series by dividing the normalized luminescence values by those obtained for the untreated control. For calibration curves, induction factors were plotted against their corresponding $ZnCl_2$ concentrations, and the best time series (580 min in the present experiment) was identified as presenting the best linear regression from which the equation connecting induction factor and bioavailable Zn^{2+} was extracted for further calculation at the corresponding time.

2.7. Instrument

Transmission electron microscopy (TEM) images were taken by placing a drop of the particles in water onto a carbon film-supported copper grid. Samples were studied using a Philips CM20 instrument operating at 200 kV. The x-ray powder diffraction diagrams of all samples were measured using Panalytical X'Pert Pro MPD diffractometer using Cu Kα radiation. The average particle size was calculated from line broadening using the Topas application (Bruker XAS). We used the fundamental parameters approach (FP) [40] and the instrumental broadening was determined using standard LaB_6 powder. The x-ray powder diffraction data were collected from an X'Pert MPD diffractometer (Panalytical AXS) with a goniometer radius 240 mm, fixed divergence slit module (1/2° divergence slit, 0.04 rad Sollers slits), and an X'Celerator as a detector. The powder samples were placed on zero-background quartz sample holders and the XRD patterns were recorded at room temperature using Cu Kα radiation ($\lambda = 0.154\,18$ nm).

Absorption spectra were recorded on a Perkin-Elmer (Lambda 2) UV–vis spectrophotometer. Fluorescence spectra were recorded on a fluorolog-3 spectrofluorimeter F222 (Jobin Yvon) using a 450 W xenon lamp. The QY values were determined from the following equation:

$$\mathrm{QY(sample)} = \left(\frac{F_{\mathrm{sample}}}{F_{\mathrm{ref}}}\right)\left(\frac{A_{\mathrm{ref}}}{A_{\mathrm{sample}}}\right)\left(\frac{n^2_{\mathrm{sample}}}{n^2_{\mathrm{ref}}}\right)\mathrm{QY}_{(\mathrm{ref})} \quad (1)$$

where F, A, and n are the measured fluorescence (area under the emission peak), absorbance at the excitation wavelength, and refractive index of the solvent respectively.

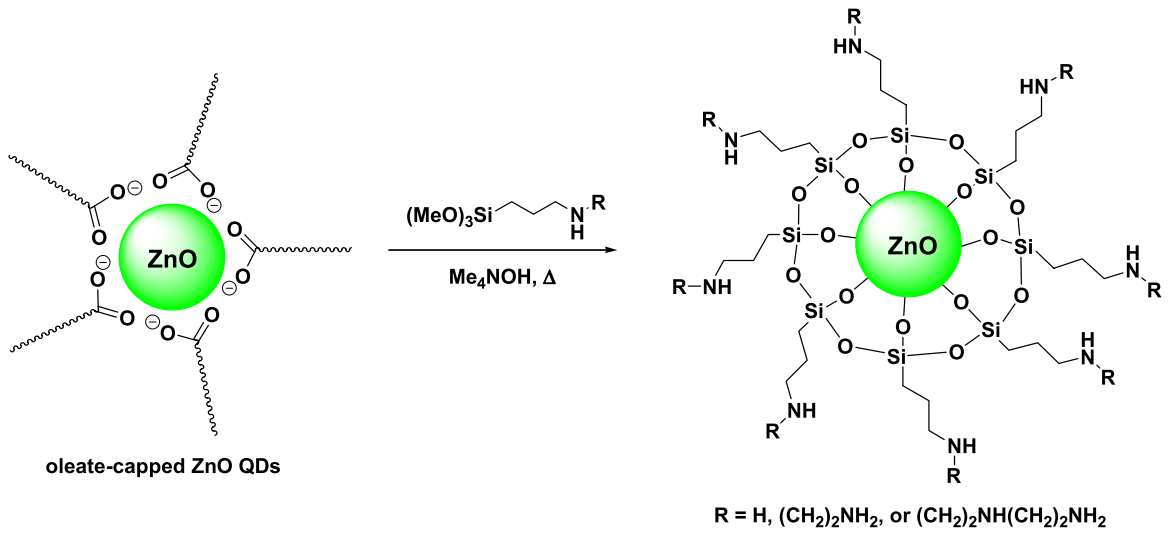

Figure 2. Synthesis of (poly)aminosilane-capped ZnO QDs.

PL spectra were spectrally corrected and quantum yields were determined relative to rhodamine 6G in ethanol (QY = 94%) using the procedure recently developed by Grabolle *et al* [41].

FT-IR spectra were recorded on a Thermo-Nicolet 5700 spectrometer equipped with the Smart Orbit diamond ATR (Attenuated Total Reflexion) accessory. Thirty-two scans were collected at 4 cm^{-1} resolution. Dynamic light scattering (DLS) was performed at room temperature using a Malvern zetasizer HsA instrument with a He–Ne laser (4×10^{-3} W) at 633 nm. The QDs aqueous dispersions were filtered through Millipore membranes (0.2 μm pore size). The data were analyzed by the CONTIN method to obtain the hydrodynamic diameter (d_H) and the size distribution in each aqueous dispersion of nanoparticles. A VARIAN 720-ES inductively coupled plasma-optical emission spectrometer (ICP-OES) was used for multielemental analyses. XPS measurements were performed at a residual pressure of 10^{-9} mbar, using a KRATOS Axis Ultra electron energy analyser operating with an Al Kα monochromatic source.

3. Results and discussion

In this work, we report a nanoparticle surface modification strategy to achieve water-dispersible amino-functionalized ZnO QDs [35, 36]. Using TEM, starting hydrophobic oleate-capped ZnO QDs appear spherical in shape and quite uniform in size (average diameter of 4.4 ± 0.6 nm, figure S1 in the supporting information available at stacks.iop.org/Nano/23/335101/mmedia). The fluorescence emission spectrum of the oleate-capped ZnO QDs is shown in figure S2 (available at stacks.iop.org/Nano/23/335101/mmedia). The sample exhibits a broad emission peak centered at 550 nm (full-width-at-half-maximum of about 130 nm). The $Zn(OH)_2$ shell coating the surface of oleate-capped ZnO QDs was used for their silanization [42]. The silanization process involves the addition of the $Zn(OH)_2$ shell to the trimethoxysilane group of APTMS, AEAPS, or AETPE. These silane agents form a Zn–O–Si covalent bond at the nanoparticles' surface and introduce respectively 1, 2, or 3 amine groups per APTMS, AEAPS, or AETPE unity at the periphery of QDs. The aminotrimethoxysilanes were added to the solution of ZnO QDs dispersed in toluene in the presence of 3 equiv. TMAH relative to the aminosilane to hydrolyze the trimethoxysilane function and initiate the surface functionalization of the dots. The three aminosilanes were condensed using the same synthetic protocol, leading to a cross-linked shell that possesses outwardly directed amine groups (figure 2). Using 0.16 equiv. aminosilanes relative to oleate-capped ZnO QDs and heating at 85 °C, the siloxane-capped ZnO QDs began precipitating within 5 min, and the precipitation was completed within 30–45 min. Interparticle cross-linking by free silane functions or formation of polysiloxanes by homocoupling was not observed by further heating at 85 °C, indicating that optimal condensation conditions were used for the surface functionalization of ZnO QDs.

We have measured the number of primary amine groups per nanocrystal using ninhydrin. Ninhydrin reacts with NH_2 functions in water at 90 °C to give a purple adduct which strongly absorbs at 570 nm [37]. Our measurements reproducibly yield 3.4 primary amine groups per nm^2 for ZnO@APTMS QDs, 2.2 for ZnO@AEAPS QDs, and 1.0 for ZnO@AETPE QDs. These values do not vary with time over a period of one month. It can be seen that the number of detectable primary amine groups at the periphery of the nanoparticles decreases with increasing the steric hindrance of the aminosilane. These values are in good accordance with those obtained from inductively coupled plasma-optical emission spectrometry (ICP-OES) measurements. The ratios of Zn/Si were found to be 2.63, 6.73, and 10.21 for ZnO@APTMS, ZnO@AEAPS, and ZnO@AETPE QDs, respectively, thus confirming that ZnO QDs were covered by about 2.5-fold less AEAPS and 3.9-fold less AETPE ligand than by the APTMS ligand. These results show that AETPE molecules pack less densely than the smaller AEAPS and APTMS ligands on the QD surface, probably due to its steric

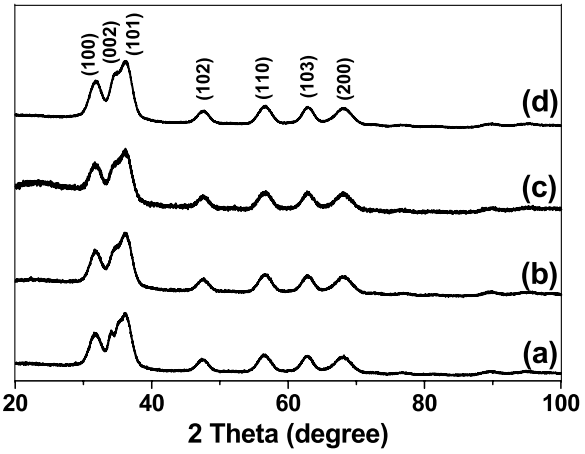

Figure 3. XRD patterns of ZnO QDs functionalized with (a) oleate, (b) APTMS, (c) AEAPS, and (d) AETPE.

hindrance and to the greater electrostatic repulsion between positively charged ammonium groups between ligands.

The electrical potential, referred to as the zeta ζ potential, which controls the colloidal stability and interparticle interactions, was also measured. At pH = 7.0, the ζ value measured for ZnO@APTMS QDs (+27.4 ± 4 mV) confirmed the presence of positive charges on the surface of QDs, due to the ammonium end group of the APTMS ligand. Increases of ζ potential values were observed for ZnO QDs functionalized with AEAPS and AETPE ligands (+31.7 ± 3 mV and +37.3 ± 4 mV, respectively) due to the presence of two and three positive charges for these ligands. These ζ potential measurements are in reasonable agreement with those described in the literature for aminosilane-capped ZnO nanocrystals [21].

Typical x-ray diffractometry (XRD) patterns of the samples before and after surface functionalization with (poly)aminosilanes are shown in figure 3. The appearance of diffraction peaks corresponding to (100), (002), (101), (102), (110), (103), and (200) planes indicates the hexagonal wurtzite structure ($P6_3mc$, $a = b = 0.325\,39$ nm, $c = 0.520\,98$ nm, JCPDS Card No. 80-0075) of ZnO QDs. The broadening of the ZnO peaks is due to the small particle size. Compared with the standard diffraction patterns, no characteristic peaks from impurities are detected, indicating the high purity of the products. Figure S3 (available at stacks.iop.org/Nano/23/335101/mmedia) shows the Rietveld refinements using the Fundamental Parameters approach built in the Topas application (Bruker XAS). A crystallite size of 5.2 ± 1.0 nm is given.

The average particle sizes were also estimated using TEM and the values are consistent with those derived from XRD peaks. Figure 4 shows TEM images of the ZnO QDs after surface functionalization and the corresponding histograms. TEM analyses indicate that all (poly)aminosilane-capped ZnO QDs have an average diameter of about 4.0 nm (table 1), which is in good accordance with the size determined for the starting oleate-capped ZnO QDs (4.4 ± 0.6 nm). Crystalline and well-separated spheroid/ellipsoid particles can be discerned. The selected area electron diffraction (SAED) patterns of the ZnO QDs functionalized with AETPE were also determined, and the results are shown in figure S4 (available at stacks.iop.org/Nano/23/335101/mmedia). All the diffraction rings can be ascribed to ZnO with a wurtzite structure.

Confirmation of particles' surface modification was attained via FT-IR (figure 5) and x-ray photoelectron spectroscopy (XPS) (figure S5 available at stacks.iop.org/Nano/23/335101/mmedia). The typical IR absorption peak of

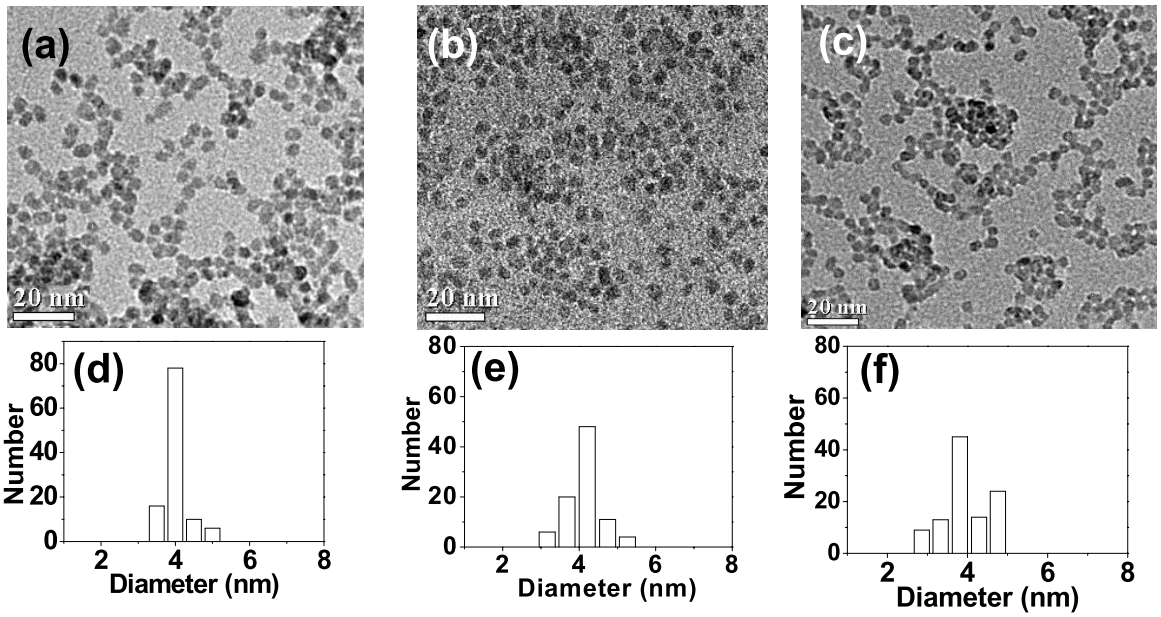

Figure 4. Typical TEM micrographs of (a) ZnO@APTES, (b) ZnO@AEAPS, and (c) ZnO@AETPE QDs showing nanoparticles of around 4 nm (about 100 particles counted), and (c)–(e) the corresponding histograms.

Table 1. TEM and DLS diameter of oleate-capped ZnO, ZnO@APTMS, ZnO@AEAPS, and ZnO@AETPE QDs.

	TEM crystallite size[a] (nm)	DLS particle size in water (nm)	DLS particle size in MOPS buffer (nm)
Oleate-capped ZnO	4.4 ± 0.6	—	—
ZnO@APTMS	4.1 ± 0.4	8.7 ± 3	12.0 ± 4
ZnO@AEAPS	4.5 ± 0.5	9.1 ± 3	14.5 ± 2
ZnO@AETPE	4.2 ± 0.4	10.5 ± 4	15.3 ± 4

[a] 100 nanoparticles were counted in TEM micrographs to determine average particle diameters.

ZnO is found at about 470 cm^{-1} in all three samples. The broad band centered at about 3395 cm^{-1} is assigned to the O–H stretching mode of surface hydroxyl groups, to the N–H stretching vibration of amino groups present in the ligand, and probably to water molecules adsorbed on the surface of nanocrystals. The peaks located at 2942 and 2857 cm^{-1} are due to symmetric and asymmetric C–H stretching vibrations of CH_2 groups. It is also found that the FT-IR spectra of ZnO QDs exhibit absorptions at 960 and 867 cm^{-1}, which could be ascribed to the characteristic peaks of Zn–O–Si and Si–O–Si symmetrical stretching vibrations, respectively. These peaks indicate that ZnO QDs are connected to the aminosilane ligands through covalent chemical bonds. The XPS scan survey spectrum of the samples show only the peaks of Zn, O, Si, N, and C elements and no peaks of any other elements were observed. As seen in figure S5(b) (available at stacks.iop.org/Nano/23/335101/mmedia) for ZnO@APTMS QDs, the peak of Zn 2p3/2 appears at 1021.2 eV, confirming that the Zn element exists only in the form of Zn^{2+} linked to an oxygen atom. Figure S5(c) (available at stacks.iop.org/Nano/23/335101/mmedia) shows that the O 1s peak is somewhat asymmetric, suggesting that there are at least three kinds of oxygen species on the sample surface. The deconvoluted peaks at about 527.9, 531.3, and 534.2 eV can respectively be attributed to the lattice oxygens of ZnO, to the oxygens of the surface hydroxyl groups, and to the oxygen atoms linked to Si. Finally, the N 1s signal (figure S5(d) available at stacks.iop.org/Nano/23/335101/mmedia) shows a main component at 399.5 eV corresponding to the primary nitrogen atoms.

The colloidal stability of (poly)aminosilanes-capped ZnO QDs in aqueous medium was also investigated. Dispersed in water at pH = 7.0 and at a concentration of 1 mg ml^{-1}, the colloidal stability of ZnO@APTMS, ZnO@AEAPS, and ZnO@AETPE QDs was found to be similar. DLS measurements (table 1) indicate only isolated nanoparticles with a hydrodynamic diameter d_H of about 10 nm. This value remained stable over three weeks at room temperature. In a higher ionic strength medium like the 3-(*N*-morpholino)propanesulfonic acid (MOPS) medium used for cytotoxicity studies (vide infra), hydrodynamic diameters of ZnO QDs measured about 2 h after dispersion of the dried powders were found to be slightly higher than those measured in water (about 13 nm, table 1). In the MOPS medium, aggregates with an average hydrodynamic diameter of 120 nm started to form about four days after the dispersion of ZnO@APTMS QDs. This phenomenon is far less pronounced for ZnO@AEAPS and ZnO@AETPE QDs and aggregates with hydrodynamic diameters of about 160 nm

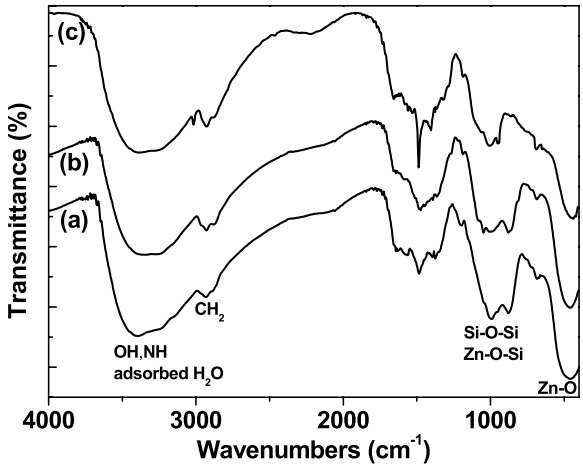

Figure 5. FT-IR spectra of (a) ZnO@APTMS, (b) ZnO@AEAPS, and (c) ZnO@AETPE QDs.

appear only the third week after the dispersion. These results tend to demonstrate the crucial role of the (poly)amino arm on the stability of ZnO QDs in aqueous medium, with longer aminosiloxane ligands providing a better stability.

In addition to the question of stability, there is the question of which siloxane ligand yields ZnO QDs with the highest or lowest PL QY. Figure 6 shows the UV–vis absorption spectra of the ZnO nanoparticles measured as colloidal solutions prepared by dispersing the (poly)aminosilanes-capped ZnO QDs in water. The absorption spectra are characteristic of ZnO nanoparticles in the quantum size regime as the excitonic absorption is markedly blue shifted in comparison with bulk ZnO (375 nm, 3.37 eV at room temperature). The relatively sharp onset of the absorption suggests a narrow size distribution. The observed excitonic absorption is at 339 nm (3.65 eV). Equation (2) shows the relationship between the radius R of spherical nanocrystals and their band gap E based on the effective mass model approximation [43, 44],

$$E = E_g + \frac{\hbar^2 \pi^2}{2R^2}\left(\frac{1}{m_e} + \frac{1}{m_h}\right) - \frac{1.8e^2}{\varepsilon R} \qquad (2)$$

where E_g is the band gap of the bulk material (3.3 eV), $\hbar$ is the reduced Planck's constant, e is the charge of the electron, ε is the semiconductor dielectric constant, m_e and m_h are effective masses of the electrons and holes, respectively, and m_o is the free electron mass. With the effective masses of electrons ($m_e = 0.26m_o$) and holes ($m_h = 0.59m_o$), a

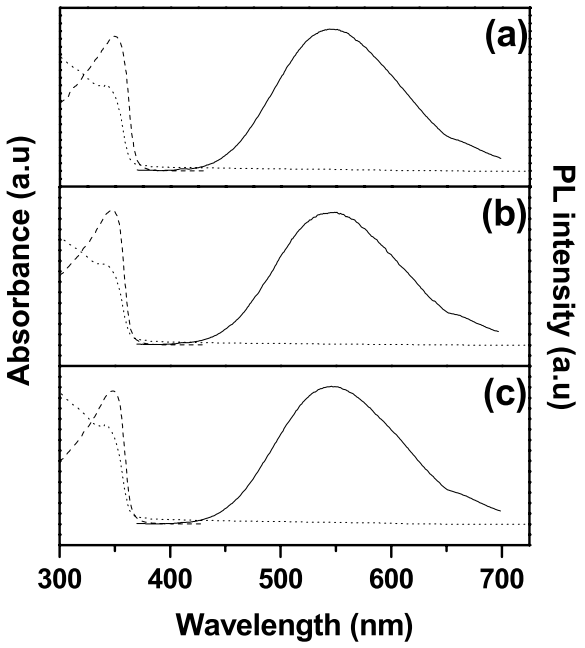

Figure 6. Normalized absorption (dotted line), PL excitation (dashed line), and PL emission (solid line) of (a) ZnO@APTES, (b) ZnO@AEAPS, and (c) ZnO@AETPE QDs dispersed in water. PL emission spectra were recorded after excitation at 350 nm.

diameter of 4.6 nm was found for ZnO QDs capped with (poly)aminosilanes. This result is in good agreement with the diameters obtained from the XRD and TEM data.

All photoluminescence (PL) excitation spectra recorded for an emission wavelength of 550 nm display a similar shape and present a strong absorption below 350 nm (figure 6). This corresponds to the transition between the valence and the conduction band which has previously been observed in the absorption spectra. The room temperature PL spectra of freshly water dispersed ZnO QDs exhibit intense and yellow emission centered at about 550 nm (2.25 eV) upon excitation at 350 nm. This yellow emission is generally considered as originating from intrinsic defects of nanocrystals such as oxygen vacancies, zinc interstitials, zinc vacancies, antisite oxygen, donor–acceptors pairs, and surface defects [45–49]. The full-width-at-half-maximum of PL spectra is about 120 nm. The PL QYs of ZnO@AETPE, ZnO@AEAPS, and ZnO@APTMS QDs measured immediately after dispersion in water and determined using rhodamine 6G in ethanol as [41], were found to be 17, 7.8, and 5.6%, respectively.

The PL stability of ZnO@AETPE, ZnO@AEAPS, and ZnO@APTMS QDs was studied by dispersing the nanoparticles in water and monitoring the change in PL intensity after excitation at 350 nm as a function of time using rhodamine 6G as reference (figure S6 available at stacks.iop.org/Nano/23/335101/mmedia). No noticeable changes in the absorption and PL emission spectra (both shape and position) of ZnO QDs were observed even after being stored in water at room temperature under atmospheric conditions over 20 days. PL QYs remained stable during the 12 first days of storage (figure S6 available at stacks.iop.org/Nano/23/335101/mmedia). PL QYs of ZnO@AETPE and

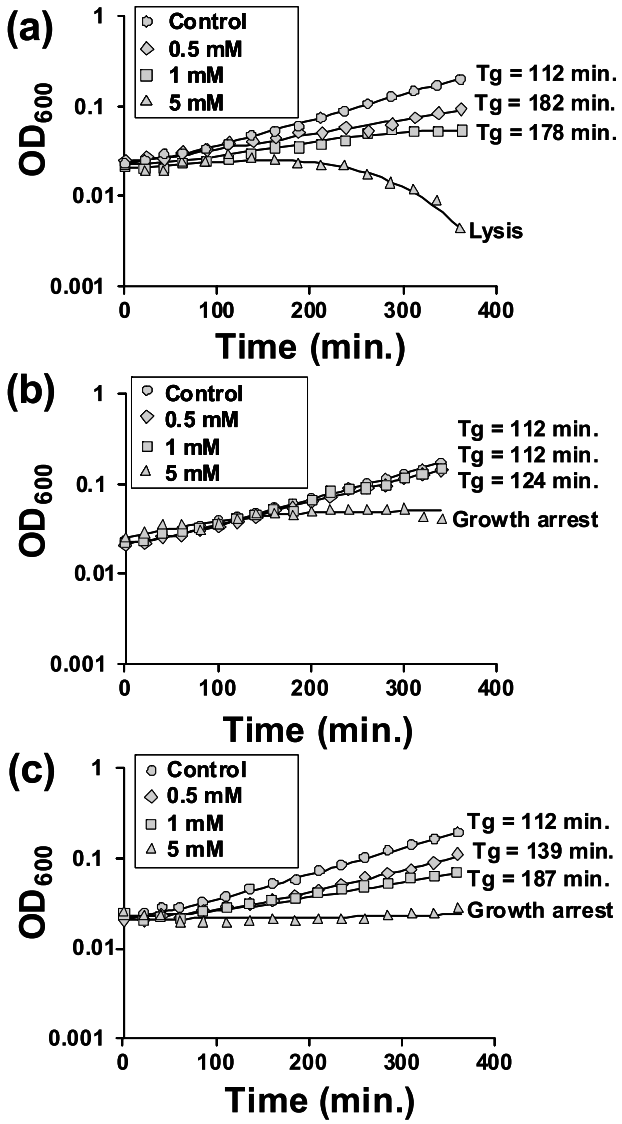

Figure 7. Growth of *E. coli* MG1655 exposed to ZnO QDs functionalized with (a) APTMS, (b) AEAPS, and (c) AETPE. MG1655 was cultivated in RM medium until OD_{600} reached 0.2 and was then diluted in the same medium supplemented with various concentrations of ZnO QDs.

ZnO@AEAPS QDs gradually decrease after 16 days of storage.

To use ZnO QDs in bio-imaging or sensing applications, the dots do not only require good optical properties, but also a low cytotoxicity. To test the correlation between cell viability and the dosage of siloxane-capped ZnO QDs, the three QDs were diluted to three different concentrations (0.5, 1.0, and 5.0 mM in cell culture medium) and incubated with *E. coli* growing cells (figure 7). For the three QDs, the toxicity was already visible at 1 mM with a slight increase of the culture doubling time. At 5 mM, bacterial division was completely inhibited and appeared as growth arrest for the three QDs. The growth inhibition test was repeated in similar conditions confirming a slower growth rate at [QDs] = 1 mM for the three nanocrystals and a complete growth arrest at [QDs] = 10 mM (data not shown).

Since the cytotoxicity of ZnO QDs may be due, at least partially, to the release of Zn^{2+} ions, it should be greatly dependent on their surface capping. Recent toxicological studies have demonstrated that uncapped ZnO nanoparticles (50–150 nm in size) exhibit strong cytotoxic effects towards gram-positive and, to a lesser extent, gram-negative bacteria. Zn^{2+} ions originating from the dissolution of ZnO nanoparticles in the biological medium were found to be at the origin of the toxicity observed [50–53]. For siloxane-capped ZnO QDs, the leakage of Zn^{2+} atoms is directly linked to the permeability of coating materials to protons who can lead to the detachment of the siloxane layer from the QD surface, followed by aggregation of QDs as well as to the dissolution of the ZnO core. In eukaryotic cells for instance, Zn^{2+} released can bind to the thiol groups of mitochondria proteins, leading to cell poisoning. For small nanoparticles like ZnO QDs with a diameter of 4.0 nm, the number of Zn–O pairs at the nanocrystal surface can be roughly estimated to be 37% using the equation:

$$\frac{N_{\text{surf}}}{N_{\text{vol}}} \approx \frac{(SR_0)}{(V - SR_0)} = \frac{3R_0}{R - 3R_0} \tag{3}$$

where N_{surf} and N_{vol} are the number of the Zn–O pairs at the surface and in the volume, respectively, S and V are the QD surface and volume, respectively, R is the particle radius, and R_0 is the Zn–O distance (0.18 nm) [54].

Since ZnO QDs present a high surface area, that about 37% of Zn–O pairs are located at the periphery of the nanocrystals, and that ZnO nanoparticle dissolution is size-dependent [55, 56], Zn^{2+} ions originating from the dissolution of ZnO QDs in the biological medium could be at the origin of the cytotoxicity observed.

Bioavailable Zn^{2+} ions leaked from ZnO QDs were quantified using the Zn^{2+} whole cell biosensor AE1433 in which a bioluminescence is specifically induced by intracellular metal ions. The recombinant *Cupriavidus metallidurans* AE1433 contains the *luxCDABE* bioluminescent genes downstream of a responding Zn^{2+} ion promoter. The response of the biosensor to bioavailable Zn^{2+} was expressed as increased induction (folds) of luminescence compared to the background values. Zn^{2+} from $ZnCl_2$ was considered 100% bioavailable and used as standards (figure 8(a)).

As shown in figure 8(b), APTMS-functionalized QDs appeared to produce 1.5–2 times more bioavailable Zn^{2+} than AEAPS and AETPE QDs for equivalent concentrations. For a QD concentration of 0.5 mM, which corresponds to the first appearance of cytotoxic effects in growth inhibition tests, the concentrations of bioavailable Zn^{2+} were estimated to reach 44, 27, and 32 μM for APTMS-, AEAPS-, and AETPE-capped QDs, respectively. Control growth inhibition tests carried out with $ZnCl_2$ as toxicant showed that inhibition could only be obtained past 100 μM. Considering the lower concentration of bioavailable Zn^{2+} delivered by the three QDs when added at 0.5 mM (early cytotoxicity), it can be concluded that zinc leaks from the core do not seem to be the primary source of toxicity observed for siloxane-capped ZnO QDs.

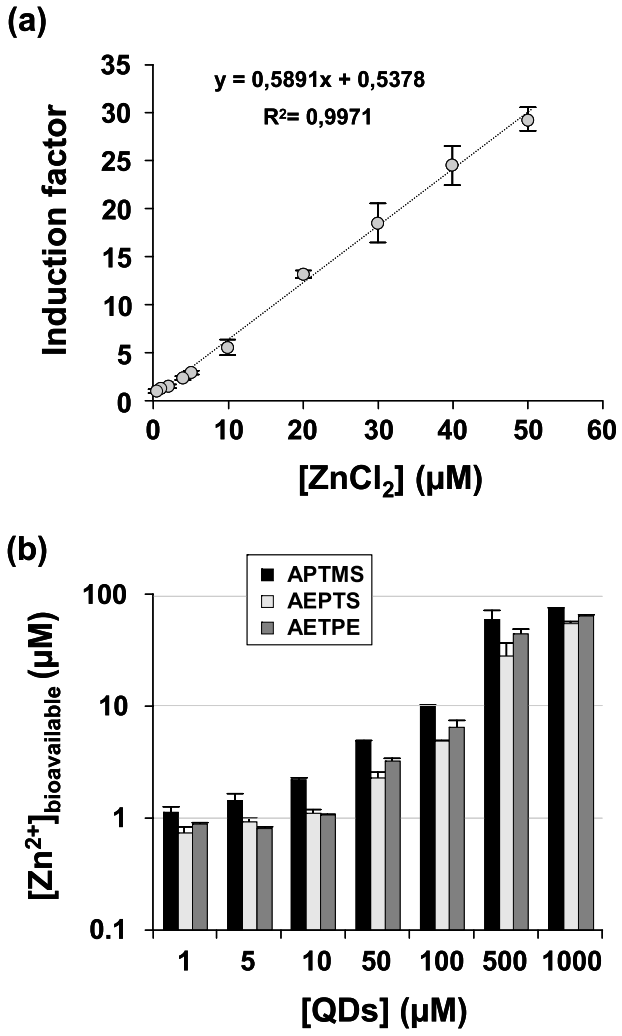

Figure 8. Bioavailable Zn^{2+} release by aminosiloxane-capped ZnO QDs measured with biosensor AE1433. (a) Calibration curve used to determine the correspondence between the induction of bioluminescence and the concentration of bioavailable Zn^{2+}. (b) Bioavailable Zn^{2+} released by the aminosiloxane-capped ZnO QDs at different concentrations. For the highest concentration of APTMS-QD, $[Zn^{2+}]$ may slightly be minimized as a consequence of an early toxic effect inhibiting the biosensor response. All data points are average values of two duplicate experiments where error bars represent deviations from the mean. Similar results were obtained in duplicate experiments.

4. Conclusions

In summary, we have reported the synthesis of water-dispersible ZnO QDs capped by (poly)aminosilanes. The dots have an average diameter of about 4 nm, exhibit strong yellow emission upon UV light excitation, and show relatively good photoluminescence quantum yields in water. Aminosilane-capped ZnO QDs have a good colloidal stability and retain their optical properties for at least 14 days while dispersed in water.

Because of their low cytotoxicity and because the large number of functional amine groups are easy to tailor, aminosiloxane-capped ZnO QDs may offer a great potential as fluorescent probes in bio-imaging. Several interesting

implications of ZnO QDs dissolution in biological medium and cytotoxicity are also obtained from this study. Firstly, the siloxane shell seems to prevent the ZnO core from complete dissolution. Secondly, the early toxic effect observed for ZnO QDs at concentrations between 0.5 and 1 mM could not be entirely attributed to metal leakage because the amounts of dissolved Zn^{2+} ions detected by the sensor bacteria *C. metallidurans* AE1433 are too low to fully explain the inhibition caused by ZnO QDs to bacteria cell growth. Additional mechanistic studies are needed to conclusively demonstrate the crucial role of oxidative stress on ZnO QDs-induced cytotoxicity.

Acknowledgments

This work is supported by the Agence Nationale pour la Recherche (ANR CESA 2011, project NanoZnOTox). The authors thank Hervé Marmier (Université de Lorraine, LIMOS, UMR CNRS 7137) for ICP-OES measurements.

References

[1] Bruchez M, Morrone P, Gin S, Weiss S and Alivisatos A P 1998 *Science* **281** 2013
[2] Chan W C and Nie S 1998 *Science* **281** 2016
[3] Zheng Y G, Gao S and Ying J Y 2007 *Adv. Mater.* **19** 376
[4] Deng Z, Zhang Y, Yue J, Tang F and Wie Q 2007 *J. Phys. Chem.* B **111** 12024
[5] Klimov V I, Mikhailovsky A A, Xu S, Malko A, Hollingsworth J A, Leatherdale C A, Eisler H J and Bawendi M G 2000 *Science* **290** 314
[6] Sun Q, Wang Y A, Li L S, Wang D Y, Zhu T, Xu J, Yang C H and Li Y F 2007 *Nature Photon.* **1** 717
[7] Medintz I L, Uyeda H T, Goldman E R and Mattoussi H 2005 *Nature Mater.* **4** 435
[8] Rogach A L, Kornowski A, Karshaw S V, Brot M, Harrison M, Eychmüller A and Weller H 1999 *Adv. Mater.* **11** 552
[9] Rogach A L, Kornowski A, Gao M, Eychmüller A and Weller H 1999 *J. Phys. Chem.* **103** 3065
[10] Peng Z and Peng X 2001 *J. Am. Chem. Soc.* **123** 183
[11] Talapin D V, Rogach A L, Shevchenko E V, Kornowski A, Haase M and Weller H 2002 *J. Am. Chem. Soc.* **124** 5782
[12] Yu W W, Wang Y A and Peng X 2003 *Chem. Mater.* **15** 4300
[13] Aboulaich A, Balan L, Ghanbaja J, Medjahdi G, Merlin C and Schneider R 2011 *Chem. Mater.* **23** 3706
[14] Aldeek F, Balan L, Medjahdi G, Roques-Carmes T, Malval J-P, Mustin C, Ghanbaja J and Schneider R 2009 *J. Phys. Chem.* C **113** 19458
[15] Schneider R, Wolpert C, Guilloteau H, Balan L, Lambert J and Merlin C 2009 *Nanotechnology* **20** 225101
[16] Dumas E, Gao C, Suffern D, Bradforth S E, Dimitrijevic N M and Nadeau J L 2010 *Environ. Sci. Technol.* **44** 1464
[17] Djurisic A B and Leung Y H 2006 *Small* **2** 944
[18] Klingshirn C 2007 *Phys. Status Solidi* b **244** 3027
[19] Tamar A, Gong Y, Polking M, Yin M, Igor K, Gertrude N and Stephen O B 2005 *J. Phys. Chem.* B **109** 14314
[20] Narayanaswamy A, Xu H, Pradham N, Kim M and Peng X 2006 *J. Am. Chem. Soc.* **128** 10310
[21] Jana N R, Yu H, Ali E M, Zheng Y and Ying J Y 2007 *Chem. Commun.* 1406
[22] Xiong H-M, Xu Y Q-G, Ren Q-G and Xia Y-Y 2008 *J. Am. Chem. Soc.* **130** 7522
[23] Zhang P and Liu W 2010 *Biomaterials* **31** 3087
[24] Joshi P, Ansari Z A, Singh S P and Shanker V 2009 *Adv. Sci. Lett.* **2** 360
[25] Tang X, Guang Choo E S, Li L, Ding J and Xue J 2010 *Chem. Mater.* **22** 3383
[26] Grasset F, Saito N, Li D, Park D, Sakaguchi I, Ohashi N, Haneda H, Roisnel T, Mornet S and Duguet E 2003 *J. Alloys Compounds* **360** 298
[27] Bruce I J and Sen T 2005 *Langmuir* **21** 7029
[28] Jana N R, Earhart C and Ying J Y 2007 *Chem. Mater.* **19** 5074
[29] Wu Y L, Tok A I Y, Boey F Y C, Zeng X T and Zhang Y H 2007 *Appl. Surf. Sci.* **253** 5473
[30] Allen C G, Baker D J, Albin J M, Oertli H E, Gillaspie D T, Olson D C, Furtak T E and Collins R T 2008 *Langmuir* **24** 13393
[31] Soares J W, Whitten J E, Oblas D W and Steeves D M 2008 *Langmuir* **24** 371
[32] Petoral R M, Yazdi G R, Spetz A L, Yakimova R and Uvdal K 2007 *Appl. Phys. Lett.* **90** 223904
[33] Li H, Zhang J, Zhou X, Lu G, Yin Z, Li G, Wu T, Baey F, Venkatraman S S and Zhang H 2010 *Langmuir* **26** 5603
[34] Selegard L, Khranovskyy V, Söderlind F, Vahlberg C, Ahren M, Käll P-O, Yakimova R and Urdal K 2010 *Appl. Mater. Interfaces* **2** 2128
[35] Moussodia R-O, Balan L and Schneider R 2008 *New J. Chem.* **32** 1388
[36] Moussodia R-O, Balan L, Merlin C, Mustin C and Schneider R 2010 *J. Mater. Chem.* **20** 1147
[37] d'Orlyé F, Varenne A, Georgelin T, Siaugue J-M, Testa B, Descroix S and Gareil P 2009 *Electrophoresis* **30** 2572
[38] Corbisier P *et al* 1999 *Anal. Chim. Acta* **387** 235
[39] Mergeay M, Nies D, Schlegel H G, Gerits J, Charles P and Van Gijsegem F 1985 *J. Bacteriol.* **162** 328
[40] Cheary R W, Coelho A A and Cline J P 2004 *J. Res. Natl Stand. Technol.* **109** 1
[41] Grabolle M, Spiles M, Lesnyak V, Gaponik N, Eychmüller A and Resch-Genger U 2009 *Anal. Chem.* **81** 6285
[42] Zhou H, Alves H, Hofmann D M, Meyer B K, Kaczmarczyk G, Hoffmann A and Thomsen C 2002 *Phys. Status Solidi* **229** 825
[43] Koch U, Fojtik A, Weller H and Henglein A 1985 *Chem. Phys. Lett.* **122** 507
[44] Brus L E 1986 *J. Phys. Chem.* **90** 2555
[45] Djuris A B, Choy W C H, Roy V A L, Leung Y H, Kwong C Y, Cheah K W, Rao T K G, Chan W K, Lui H F and Surya C 2004 *Adv. Funct. Mater.* **14** 856
[46] Xiong H, Wang Z, Liu D, Chen J, Wang Y and Xia Y 2005 *Adv. Funct. Mater.* **15** 1751
[47] Djuris A B and Leung Y H 2006 *Small* **2** 944
[48] Reschikov M A, Morkoc H, Nemeth B, Nause J, Xie J, Hertog B and Osinsky A 2007 *Physica* B **401/402** 358
[49] Zhang L, Yin L, Wang C, Iun N, Qi Y and Xiang D 2010 *J. Phys. Chem.* C **114** 9651
[50] Kasemets A, Ivask A, Dubourguiev H-C and Kahru A 2009 *Toxicol. in Vitro* **23** 1116
[51] Xia T, Kovochich M, Liong M, Mädler L, Gilbert B, Shi H, Yeh J I, Zink J I and Nel A E 2008 *ACS Nano* **2** 2121
[52] Song W, Zhang J, Guo J, Zhang J, Ding F, Li L and Sun Z 2010 *Toxicol. Lett.* **199** 389
[53] Huang Z, Zheng X, Yan D, Yin G, Liao X, Kang Y, Yao Y, Huang D and Hao B 2008 *Langmuir* **24** 4140
[54] Monticone S, Tufeu R and Kanaev A V 1998 *J. Phys. Chem.* B **102** 2854
[55] Meulenkamp E A 1998 *J. Phys. Chem.* B **102** 7764
[56] Mudunkotowa I A, Rupasinghe T, Wu C-M and Grassian V H 2012 *Langmuir* **28** 396